2015

Modeling of Nitrogen Separation from Natural Gas through Nanoporous Carbon Membranes

Moustafa A. Soliman
The British University in Egypt, moustafa.aly@bue.edu.eg

A A. Al-Rabiah
King Saud University

AbdelHamid M. Ajbar
King Saud University

F A. Almalki

Omar Y. Abdelaziz

Journal of Natural Gas Science and Engineering 26 (2015) 1278–1284

Contents lists available at ScienceDirect

Journal of Natural Gas Science and Engineering

journal homepage: www.elsevier.com/locate/jngse

Modeling of nitrogen separation from natural gas through nanoporous carbon membranes

Abdulrahman A. Al-Rabiah [a, *], Abdelhamid M. Ajbar [a], Moustafa A. Soliman [a, b], Fahad A. Almalki [c], Omar Y. Abdelaziz [d]

[a] Chemical Engineering Department, King Saud University, Riyadh 11421, Saudi Arabia
[b] Department of Chemical Engineering, The British University in Egypt, El-Shorouk City, Cairo 11837, Egypt
[c] King Abdulaziz City for Science and Technology, Riyadh 11442, Saudi Arabia
[d] Department of Chemical Engineering, Cairo University, Giza 12613, Egypt

ARTICLE INFO

Article history:
Received 2 July 2015
Received in revised form
20 August 2015
Accepted 20 August 2015
Available online 25 August 2015

Keywords:
Nanoporous carbon membrane
Dusty gas model
Mathematical modeling
Nitrogen removal
Natural gas
Selective surface flow

ABSTRACT

This work presents a theoretical investigation of the use of nanoporous carbon membranes for the separation of nitrogen from natural gas. A mathematical model to predict the performance of the membrane is developed. The model is a combination of the well known dusty gas model, which describes the transfer of multi-components mixture in porous media, together with a surface diffusion model. The model is first validated using the literature results for the separation of hydrogen from hydrocarbons mixture. The model is then applied to the nitrogen-hydrocarbons system. The membrane performance is evaluated in terms of nitrogen recovery, methane loss, nitrogen purity, as well as hydrocarbons compositions in both permeate and retentate sides. The model calculation methods are applied for both co-current and counter-current flow configurations. A parametric study is also carried out to investigate the effects of membrane parameters such as feed and permeate pressures and porosity on the membrane performance. The developed model is general and can be applied to various nanoporous membrane flow patterns.

1. Introduction

Natural gas is of great importance as a primary source of energy, synthesis gas and as a raw material for petrochemical industries. Ammonia and methanol are examples of industries that benefit from the natural gas as a raw material. Most industrial specifications require no more than 4% nitrogen or total inerts in the pipelines (Baker, 2002). Large proven reserves in the world cannot be produced due to presence of high percentage levels of nitrogen gas. The Kingdom of Saudi Arabia, for instance, has one of the world's highest proven reserves of natural gas. As reported by Saudi Aramco, it is estimated at 241 trillion cubic feet, ranking fourth in the world after Russia, Iran, and Qatar (Aleklett et al., 2010). About 60% of these reserves are “associated gas” from oil fields. Most of Saudi Arabia's non-associated gas reserves contain mainly methane and a high nitrogen content that normally exceeds 14 mol %. Technology is therefore needed to economically bring the gas to pipeline quality levels.

Currently, there are essentially four possible methods available for removal of nitrogen from natural gas: cryogenic distillation, pressure swing adsorption (PSA) process, lean oil absorption processes, and membrane processes. The cryogenic process is the only process that is used nowadays on any industrial scale. PSA process is of limited commercial application, while the remaining processes are in the research stage. Cryogenic processes are typically used with large capacity applications. The process is characterized by a high methane recovery rate. However, high capital and compression costs besides the need for extensive pretreatment are major drawbacks within the process. The pretreatment consists generally of amine scrubbing in order to remove the carbon dioxide present. Next, glycol dehydration is performed to eliminate most of the water vapor. Molecular sieves afterward get rid of any carbon dioxide and water vapor left, after which the gas is chilled in a final polishing stage to eliminate heavy hydrocarbons and aromatics. The complexity of the pretreatment makes the operational reliability a concern. On another hand, methane and other hydrocarbons are commonly adsorbed onto molecular sieves in the PSA

* Corresponding author.
E-mail address: arabiah@ksu.edu.sa (A.A. Al-Rabiah).

http://dx.doi.org/10.1016/j.jngse.2015.08.040
1875-5100/

process, resulting in a nitrogen-rich gas stream (Tagliabue et al., 2009). Typically, multiple beds are employed, with complex switching controls across the beds. However, the capital and operating costs of these systems are rather high. Meanwhile, lean oil absorption processes have been under establishment for about 20 years (Yildirim et al., 2012). Such processes mostly exploit chilled oil to absorb methane and other hydrocarbons. A good recovery for hydrocarbons is attained, but the process is often considered capital intensive. Also, the requirement to absorb methane bulk further increases equipment size and compression duties. It is expected in the upcoming decades that, more efficient nitrogen removal technologies will emerge to improve the materials stability and the separation power (Rufford et al., 2012).

Membrane technology has been considered recently for gas separation (Ahmad et al., 2015; Bara et al., 2009; Cai et al., 2012; Rezakazemi et al., 2011; Saidi et al., 2014) and nitrogen removal from natural gas (Baker et al., 2003; Lokhandwala et al., 2010; Wu et al., 2015). The use of membranes offers in general a number of advantages including low capital cost, low energy use, cost effectiveness even at low gas volume, and considerable weight and space efficiency (Scholes et al., 2012). For the nitrogen removal from natural gas, either glassy polymers that are ordinarily nitrogen-permeable, or rubbery polymers that are normally methane-permeable, can be used. Ever since, these traditional polymeric membranes (glassy and rubbery) have low selectivities for nitrogen over methane and vice versa (Baker et al., 2003). On the other hand, inorganic membranes, including nanoporous membranes, have the desirability of higher permeability values comparing to polymeric membranes, and their selectivities are however high (Baker, 2002). Table 1 shows a comparison between different membrane materials that can be adopted for nitrogen removal from natural gas.

Carbon porous membranes appeared to provide added features comprising higher rates of transport, thermal stability, and high selectivity. Two types of carbon membranes have acquired much attention for gas separation: namely, molecular sieving membranes and nanoporous membranes (Seo et al., 2002). In molecular sieving membrane, the separation is based on molecular size differences (Koresh and Sofer, 1983). This kind of membranes allows passage of smaller molecules through the pores of the membrane while blocking larger molecules. The molecular sieving membranes can have high permeability and selectivity for the smaller components. Despite of that, they need delicate control of the pore sizes close to the size of the gas molecules to be separated (Seo et al., 2002). In nanoporous membranes, the pores are larger than the dimension of the molecules and the separation selectivity is determined by surface diffusion and preferential adsorption of the more strongly adsorbed species (Vieira-Linhares and Seaton, 2003). Thus, both the pore size and the nature of the surface play key roles in the membrane performance. In their pioneering work, Rao and Sircar (Rao and Sircar, 1993a) developed a nanoporous carbon membrane, which they called selective surface flow (SSF) membrane. This membrane has pore sizes typically in the range of 5–6 Å, and achieved separation on the selective adsorption basis followed by surface diffusion. Additionally, the authors went further to study the SSF membrane performance for the separation of hydrogen-hydrocarbon gas mixtures (Rao and Sircar, 1996).

Mathematical modeling of nanoporous membranes has also grabbed an increasing attention in literature (Bowen and Welfoot, 2002; Habib and Habib, 2004; Seo et al., 2002; Vieira-Linhares and Seaton, 2003; Xu et al., 2000). Such tailor-designed membranes are considered to play an important role in improving membrane systems and environment (Dionysiou, 2004). Because of the nanoscale nature of the membrane, molecular dynamics (MD) modeling and Monte Carlo (MC) simulation, have been commonly used in studying the molecular diffusion in porous medium (Seo et al., 2002; Vieira-Linhares and Seaton, 2003; Xu et al., 2000). A number of these modeling studies addressed the permeability and selectivity prediction of nanoporous carbon membranes, but there has been no report on the detailed performance study of nanoporous carbon membranes for nitrogen removal from natural gas.

The general objective of this research is to contribute to the understanding of the potential benefits of using nonporous membrane for the nitrogen removal from natural gas through the development of a mathematical model of the membrane and the determination of its performance. The model and calculation methods are presented for both co-current and counter-current flow configurations. The organization of this paper includes the presentation of the model and the solution strategy for both flow configurations, proceeding ahead to the validation of the model using the results of the pioneering work of Rao and Sircar (Rao and Sircar, 1996) for hydrogen-hydrocarbons system. This is followed by the presentation of simulation results for nitrogen-hydrocarbons system.

2. Modeling the nanoporous membrane

The model developed in this work is used to predict the transport of different species of multi-component gas mixture through the nanoporous membrane. The model includes the following transport modes that exist in porous media: (1) *Free-molecule or Knudsen flow*, where the gas density is low to the point that collisions between gas molecules can be neglected, contrasted with gas molecules collisions with the walls of porous medium. (2) *Viscous or convective or bulk flow*, where the gas performs as a continuum fluid forced by a pressure gradient, and gas–gas collisions control over gas–wall collisions. (3) *Ordinary or continuum diffusion*, to which the mixtures unlike species move relative to one another affected by concentration gradients. (4) *Surface flow or adsorption*, in which molecules move along a solid surface in an adsorbed layer (Fuertes, 2000; Rao and Sircar, 1993b). For the development of the model, we consider a similar schematic diagram for the membrane with counter-current flow used by Shindo et al. (Shindo et al., 1985), as shown in Fig. 1.

The following are the main assumptions used to derive the mathematical model:

Table 1
Comparison between different membrane materials including the nanoporous carbon membrane (Scholes et al., 2012).

Membrane material	Type	Selectivity P_{CH4}/P_{N2}
Selective surface flow (SSF)	Nanoporous inorganic	8.80
Polydimethysiloxane (PDMS)	Rubbery polymer	3.15
PTMSP	Super glassy polymer	2.44
Polyimide (6FDA-BAHF)	Glassy polymer	2.3 at P_{N2}/P_{CH4}
Polyamide-polyether block copolymer (Pebax® 2533)	Rubbery polymer	2.8 at T = 22 °C
Silicon rubber	Rubbery polymer	4

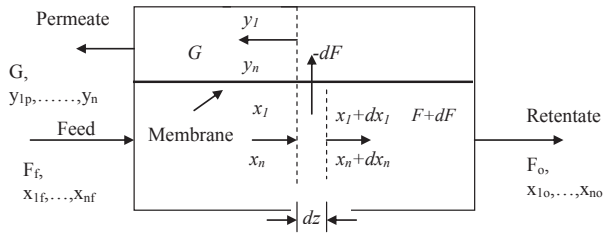

Fig. 1. Membrane flow diagram with counter-current flow.

- Plug flow conditions are assumed in the feed and permeate sides.
- Permeability is assumed to be independent of pressure and temperature for every gas component.
- The membrane thickness is assumed to be constant all over the entire length of the unit.
- Pressure drop is negligible for the feed stream as well as the permeate gas stream.
- The feed gas is assumed to consist of nitrogen and essentially the following mixture of hydrocarbons: CH_4, C_2H_6, C_3H_8 and C_4H_{10}.

The same notations that were used for the development of simple solution-diffusion model are adopted here. This approach is in good agreement and exists with prior literature results for membrane separation processes (e.g., Mulder, 1996; Rao and Sircar, 1996; Wijmans and Baker, 1995).

2.1. Model for co-current configuration

We consider the schematic diagram for a membrane (Fig. 1) but with co-current flow. The balance equations for each component (i) are given by:

$$\frac{dF_i}{dA} = -N_{T_i}, \quad F_i(0) = F_f y_i(0) \quad i = 1,2,n \tag{1}$$

$$\frac{dG_i}{dA} = N_{T_i}, \quad G_i(0) = 0 \quad i = 1,2,n \tag{2}$$

Such that F_f is the inlet feed flowrate, F_i the flowrate of component (i) in retentate, N_{T_i} the total flux through the membrane of component (i), G_i the flowrate of component (i) in the permeate, y_i the gas mole fraction at the permeate side, A_T the membrane area, and $G_i(A_T)$ the given component (i) inlet permeate side flowrate at the total area A_T (i.e. sweep gas).

The total flux (N_{T_i}) is the sum of the dusty flux (N_i) and the surface diffusion flux N_{SD_i}.

$$N_{T_i} = N_i + N_{SD_i} \tag{3}$$

The dusty gas model equations adopted are given as:

$$-\sum_{j=1}^{N}\frac{(x_j N_i - x_i N_j)}{D_{ij}} - \frac{N_i}{D_i^K} = \frac{P}{RTL}\frac{dx_i}{dz} + \frac{x_i}{RTL}\left(1 + \frac{\varepsilon}{\tau}\frac{r^2}{8}\frac{P}{\mu_i D_i^K}\right)\frac{dP}{dz} \quad i = 1,2,n \tag{4}$$

Where L is the thickness of the membrane, z the dimensionless distance through the membrane, P the total pressure inside the membrane, T the temperature, x_i the mole fraction inside the membrane, D_i^K the Knudsen diffusivity, D_{ij} the binary gas diffusivity, r the pore radius, and μ_i is the gas viscosity.

The term $\sum_{j=1}^{N}\frac{(x_j N_i - x_i N_j)}{D_{ij}}$ represents the Stefan Maxwell term (multi-component molecular diffusion), while $\frac{N_i}{D_i^K}$ is the Knudsen diffusion (molecules–wall interaction). The term $\left(\frac{\varepsilon}{\tau}\frac{r^2}{8}\frac{P}{\mu_i D_i^K}\right)\frac{dP}{dz}$ is the intra-molecular viscous friction, while the term $\left(\frac{P}{RTL}\frac{dx_i}{dz} + \frac{x_i}{RTL}\frac{dP}{dz} = \frac{1}{RTL}\frac{dPx_i}{dz}\right)$ represents the concentration gradient. The surface diffusion flux is, on another hand, given by $N_{SD_i} = -\frac{Q_i}{L}\frac{dPx_i}{dz}$ where Q_i is the permeability of component (i). To the model equations is added the consistency relation:

$$\sum_{i=1}^{N} x_i = 1 \tag{5}$$

The model equations are solved using the orthogonal collocation method (Soliman, 1992). The orthogonal collocation is applied at n_c interior collocation points inside the membrane such that:

$$\frac{dx_{i,j}}{dz} = \sum_{k=2}^{nc+1} A_{j+1,k}x_{i,k-1} + A_{j+1,1}y_i \quad j = 1,2,n_c \;\; and \;\; i = 1,2,\ldots,n \tag{6}$$

There are ($n \times n_c$)variables: $x(i + (j-1)n)$ $i = 1,2, \ldots, n$ and $j = 1,2, \ldots, n_c$ where i represents a component and j represents a collocation point. $A_{j,k}$ are the elements of $((n_c+1)(n_c+1))$ matrix of the weights of first derivative. Similarly, for the pressures:

$$\frac{dP_j}{dz} = \sum_{k=2}^{nc+1} A_{j+1,k}P_{k-1} + A_{j+1,1}P_f \quad j = 1,2,n_c \tag{7}$$

Where P_f is the pressure at feed side and $P_k = x(nn_c + k)$, $k = 1,2,..,n_c$. The mole fractions (m_i) regarding the gas at the permeate side are required to be equal to those obtained from extrapolation of the gas mole fraction at the feed side such that:

$$m_i = \sum_{k=1}^{nc+1} (X_{interp})_k x_{i,k-1} + (X_{interp})_1 y_i \quad i = 1,2,n-1 \tag{8}$$

In which that $(X_{interp})_k$ is the elements of $(n_c+1) \times 1$ vector of weights of the Lagrange interpolation formula at $z = 1$. Also, we have:

$$m_i = \frac{G_i}{\sum_{i=1}^{n} G_i} \tag{9}$$

The pressure P_p at the permeate side is, on the other hand, given by:

$$P_p = \sum_{k=2}^{nc+1} (X_{interp})_k P_{k-1} + (X_{interp})_1 P_f \tag{10}$$

We have $(n+1)n_c + n$ variables that represent the gas flux. Hence, the numbers of equations are:

- $n \times n_c$ equations of the dusty gas equations (Eq. (4)) at the collocation points.
- n_c equations of the summation equation (Eq. (5)) at n_c collocation points.
- One equation for the permeate pressure (Eq. (10)).
- $(n-1)$ equations of the combination of (Eq. (8)) and (Eq. (9)) by eliminating m_i but replacing (Eq. (9)) by:

$$m_i = \frac{N_i}{\sum_{i=1}^{n} N_i} \tag{11}$$

Consequently, this gives a total of $(n + 1)n_c + n$ equations.

For the simultaneous solution strategy, the nonlinear algebraic equation solver subroutine NEQNF in IMSL (Fortran Math Library) is used to obtain the mole fractions of the gas at the inlet of the permeate side. Having obtained the mole fractions of the gas at the permeate side inlet, we then add *2n* differential equations (Eqs. (1) and (2)) and solve the system of differential and algebraic equations using the DASSL software.

2.2. Model for the counter-current configuration

We consider the counter-current configuration of the membrane shown earlier in Fig. 1. The model equations for the co-current case hold with the exception of the following changes; Eq. (2) becomes:

$$\frac{dG_i}{dA} = -N_i \quad G_i(A_T) = 0 \quad i = 1, 2, n \tag{12}$$

For the counter-current case, the values of y_i at the exit of the retentate side (inlet of permeate side) are unknown. These should be assumed by guessing the values of $F_i(A_T)$. Again for the solution strategy, the nonlinear algebraic equations solver NEQNF from IMSL is used to obtain the gas mole fractions on the permeate side inlet. After obtaining the gas mole fractions on the permeate side inlet, we subsequently add *2n* differential equations (Eqs. (1) and (2)) and solve the system of differential and algebraic equations via the DASSL software, starting from the permeate inlet side ($A = A_T$); using the values of the assumed $F_i(A_T)$. At the exit of the retentate side ($A = 0$), a total of (n) equations must be satisfied;

$$F_i(\text{computed}) = F_i(0)(\text{given}) \tag{13}$$

These n equations in n unknowns $F_i(A_T)$ are iterated on in an external loop using NEQNF until convergence is reached.

3. Results and discussion

3.1. Validation study

The model is first solved and validated using the data pertinent to the separation of hydrogen from hydrocarbons, as reported in the experimental work of Rao and Sircar (Rao and Sircar, 1996). The nanomembrane has a thickness of 2.5 μm, a pore diameter of 5 A, a porosity of 0.36, and a tortuosity of 2. The values of Knudsen diffusivity, binary gas diffusivities, and viscosities are hence calculated (Poling et al., 2001). In the paper of Rao and Sircar, the membrane performance was evaluated in terms of hydrogen recovery, concentrations of gases in the permeate side as well as hydrocarbon rejections. The feed gas flow rate was maintained constant at 0.067 gmol/s and it consisted (in mol %) of 40% H_2, 20% CH_4, 20% C_2H_6, 10% C_3H_8, and 10% C_4H_{10}. The temperature was kept constant at 263 K while the feed pressure was varied for a counter-current configuration model. Table 2 lists the model predictions together with the experimental results for the case of a sweep gas pressure of 1.07 atm and a hydrogen sweep gas consisting of 10% of the feed flow rate. Four values of permeate pressure (P_H) were investigated as: 5.11, 4.39, 3.38 and 1.35 atm.

It can be seen from the table that, the model predictions follow the expected trend for the effect of increasing feed pressure (P_H). The hydrogen recovery in the retentate stream decreases as P_H increases, while the hydrogen composition increases. It is also noticed that the relative error between the predictions of the developed model and the experimental results is reasonable. The relative error reaches the value of around 16% for the prediction of hydrogen recovery for $P_H = 5.11$ atm, but the error is smaller (below 8%) for lower feed pressure. In a similar way, the relative error is below 7% for the predictions of hydrogen and methane compositions. As for the butane and propane, the relative error is larger. This can be attributed to the small values of their compositions.

3.2. Results for the nitrogen–natural gas separation

The validated model is then used for the investigation of membrane performance for the nitrogen separation from natural gas. The nominal feed composition consists of 100 mol/hr of a mixture of nitrogen and natural gas with the following composition: 12.9% N_2, 67.8% CH_4, 30% C_2H_6, 10% C_3H_8, and 2% n-C_4H_{10}. The temperature is assumed to be constant at 54 °C. In the first set of investigation, the flow configuration is assumed to be co-current. Table 3 summarizes the composition of the gases at the exit of the membrane.

As can be seen, the nitrogen recovery increases with permeate pressure. Nitrogen recovery is interpreted as the nitrogen fraction in the retentate stream. Starting from a value of 29.6% at a permeate pressure of 1 bar, the nitrogen recovery increases to 52.9% for a permeate pressure of 4 bar. The methane loss also increases from 21.5% to around 47.6%. The methane loss is defined as the fraction of methane in the retentate stream. Table 3 also demonstrates that the permeate stream is rich in methane, where the mole fraction reaches 77%, while the nitrogen mole fraction constitutes about 13% of the stream. Moreover, the composition of the retentate displays a rich stream in methane, where its composition increases with increasing permeate pressure. The nitrogen fraction in the retentate stream decreases, on the other hand, with the permeate pressure from 17.4% to 15.2%.

The developed model also allows a sensitivity analysis for the performance of the membrane. Fig. 2a depicts the variations of methane loss with the relative area for feed pressure of 10 bar and for different permeate pressure values 1, 2 and 4 bars.

The relative area is defined by $s = \frac{AQ_m P_H}{FL}$, where Q_m is the permeability of the base component (nitrogen). Given an assumed total area of the membrane of 20 m^2, the maximum value of the relative area is 0.0235. It can be seen from the figure that, as expected, the methane loss decreases with the relative area of the membrane. Typical values of methane loss range from 0.1 to 0.8 for relative areas in the range of 0.01–0.02. In addition, the figure shows that for a desired methane loss, an increase in the permeate pressure would require a larger relative area of the membrane. As an example, for a desired methane loss of 60%, an increase in pressure from 1 bar to 4 bar would increase the relative area from 0.012 to 0.021. Nevertheless, Fig. 2b presents the effect of permeate pressure on the nitrogen recovery and its purity. As can be noted, for a required nitrogen recovery, an increase in the permeate pressure decreases the nitrogen purity accordingly. For example, at a gas pressure of 1 bar, a recovery of 60% is associated with a nitrogen purity of 0.17%, while at larger feed pressure of 4 bar, the purity decreases to 0.14%. The effect of permeate pressure on the decrease in nitrogen purity is clearer for smaller values of nitrogen recovery.

For the same co-current configuration, Fig. 3a demonstrates the effect of increasing the feed pressure on the performance of the nanomembrane. In this context, the permeate pressure is maintained at 1 bar.

It is obvious that for the same area, an increase in the feed pressure entails a subsequent decrease in the methane loss. By way of illustration, for a relative area of 0.015, an increase in the feed pressure from 10 to 25 bar would decrease the methane loss from

Table 2
Comparison between experimental data and model predictions for the effect of feed gas pressure (sweep pressure maintained at 1.07 atm and ratio of hydrogen sweep to feed flow rate is 0.1).

Feed gas pressure (atm)	Results	H_2 recovery (%)	H_2 mol (%)	CH_4 mol (%)	C_2H_6 mol (%)	C_3H_8 mol (%)	C_4H_{10} mol (%)
5.11	Experimental	62.5	57.0	26.3	14.5	2.4	0.0
4.39		78.5	52.1	25.3	17.7	4.5	0.4
3.38		80.1	49.5	23.2	19.5	6.5	1.3
1.35		98.4	42.6	21.1	19.5	8.7	8.0
5.11	Model results	72.80	53.4	26.3	16.8	3.3	0.08
4.39		78.6	52.0	25.3	17.8	4.5	0.43
3.38		86.5	49.4	23.7	18.6	6.1	2.2
1.35		99.7	43.7	20.1	18.9	8.8	8.5
5.11	Relative error (%)	16.5	6.3	0.0	15.9	37.5	–
4.39		0.1	0.2	0.0	0.6	0.0	7.5
3.38		8.0	0.2	2.2	4.6	6.2	69.2
1.35		1.3	2.6	4.7	3.1	1.1	6.3
	Observations					Some values of relative errors are large due to small compositions	

Table 3
Effect of permeate pressure on the nanomembrane performance (Conditions of Fig. 2 at the relative area of 0.0239).

Feed pressure	Permeate pressure	N_2 recovery (%)	Methane loss (%)	Composition in permeate (%)					Composition in retentate (%)				
P^H (bar)	P^L (bar)			N_2	CH_4	C_2H_6	C_3H_8	C_4H_{10}	N_2	CH_4	C_2H_6	C_3H_8	C_4H_{10}
10	1	29.57	21.46	13.12	76.90	5.62	2.21	2.15	17.38	66.24	7.79	3.97	4.62
10	2	37.55	30.02	13.08	77.00	5.60	2.19	2.13	16.38	68.79	7.27	3.55	4.02
10	4	52.92	47.57	13.13	76.85	5.63	2.22	2.17	15.19	71.75	6.66	3.06	3.34

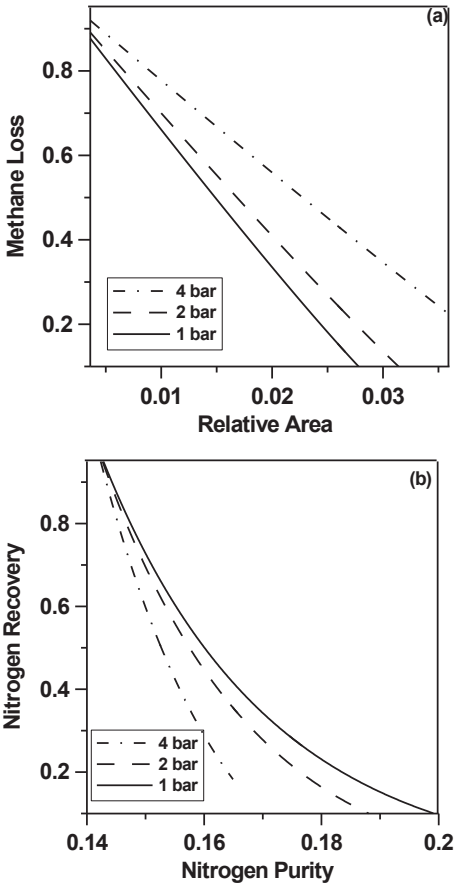

Fig. 2. Effect of permeate pressure on the nanomembrane performance. Co-current configuration. Porosity is 0.36. Feed pressure is 10 bar. Nitrogen in the feed is 14.14%.

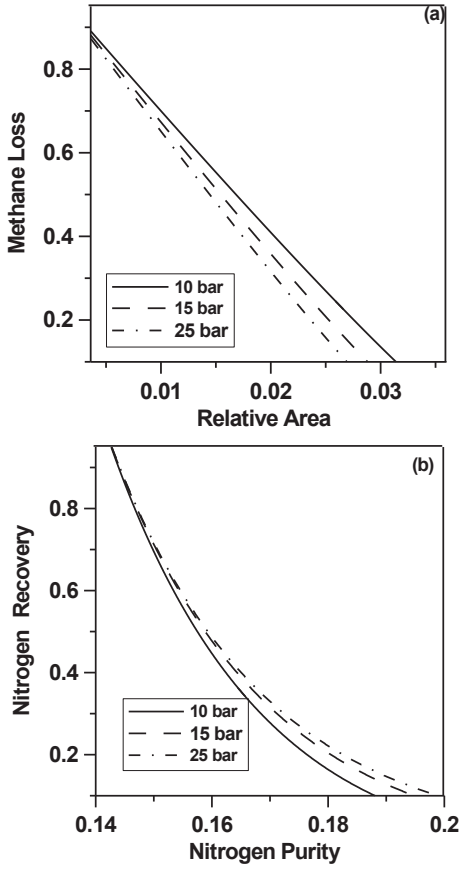

Fig. 3. Effect of feed pressure on the nanomembrane performance. Co-current configuration. Porosity is 0.36. Permeate pressure is 1 bar. Nitrogen in the feed is 14.14%.

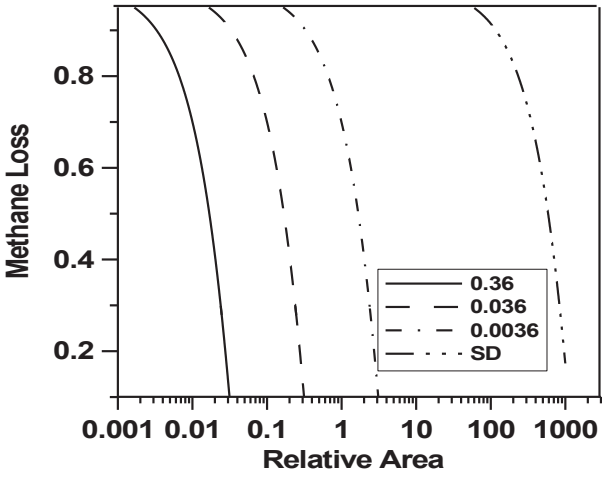

Fig. 4. Effect of porosity on the nanomembrane performance. Co-current configuration. Feed pressure is 10 bar. Permeate pressure is 2 bar. Nitrogen in the feed is 14.14%.

0.6 to 0.55. In spite of that, Fig. 3b illustrates that for desired nitrogen purity, the increase in the feed pressure increases the nitrogen recovery. Hence, for nitrogen purity of 0.14, an increase in feed pressure values from 10, 15–25 bar increases the nitrogen recovery from 0.6 to 0.61 to 0.63. The pressure increase from 15 to 25 bar is noticed to be insignificant.

The effect of porosity on the membrane performance is introduced as in Fig. 4. Smaller values of porosity would make the model approach the asymptotic simple solution-diffusion case.

It can be realized from Fig. 4 that, the porosity has a substantial effect on the performance of the membrane. To give an instance, for a desired nitrogen recovery of 80%, a decrease in the porosity from 0.36 to 0.036 increases the required relative area from 0.001 to 0.1. The asymptotic case is the solution-diffusion (SD) model where the required area would be 500% more.

Additionally, the effect of flow configuration on the membrane performance is examined. Table 4 displays the performance of the membrane for co and counter-current flow configurations. The feed pressure is adjusted at 10 bar, while the permeate feed pressure is 2 bar.

It appears that the counter-current flow yields a larger nitrogen recovery and a slightly larger methane loss. As for the permeate stream, the methane mole fraction is larger for co-current flow (77% compared to 75.62%). The nitrogen composition is, on the contrary, larger for the counter-current flow. The composition of the rest of hydrocarbons is recognized to be larger in the counter-current case. As for the composition of the retentate stream, the table shows opposite trends to the permeate stream. The methane composition is larger in counter-current, while the opposite is for nitrogen composition. Contradictorily, the rest of hydrocarbons compositions are larger for co-current flow.

Another aspect of the effect of flow configuration is illustrated in Fig. 5(a–b). The feed pressure is maintained at 10 bar and the permeate pressure at 2 bar.

It is found that for the same relative area, the counter-current

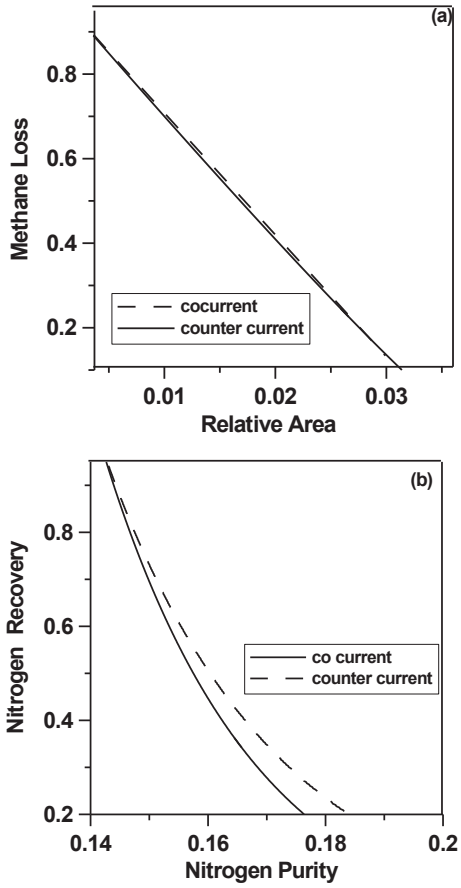

Fig. 5. Effect of flow configuration on the nanomembrane performance. Porosity is 0.36. Feed pressure is 10 bar. Permeate pressure is 2 bar. Nitrogen in the feed is 14.14%.

configuration yields relatively smaller methane loss (see Fig. 5a). For a relative area of 0.01, the methane loss is 70% with counter-current, compared to 69% for co-current configuration. Nonetheless, the effect of flow configuration is evidently clearer in Fig. 5b. It can be perceived that, for a desired nitrogen purity, the counter-current flow yields larger nitrogen recovery. In the manner that, for a nitrogen purity of 0.15, the counter-current flow configuration would yield a nitrogen recovery of 80% compared to only 79% for co-current flow. The effect of the flow configuration is more accentuated when smaller nitrogen purity (i.e. high nitrogen recovery) is sought.

4. Conclusions

This paper has developed a first principle model for the separation of gases in carbon nanomembranes. The model is based on the classical dusty gas model coupled with a simple surface diffusion model. In the first stage, the developed model was validated against the experimental work in the literature for the separation of hydrogen from hydrocarbons. The model was later used for a

Table 4
Effect of flow configuration pressure on the nanomembrane performance (Conditions of Fig. 5 at the relative area of 0.0239).

Flow configuration	N_2 recovery (%)	Methane loss (%)	Composition in permeate (%)					Composition in retentate (%)				
			N_2	CH_4	C_2H_6	C_3H_8	C_4H_{10}	N_2	CH_4	C_2H_6	C_3H_8	C_4H_{10}
Co-current	37.55	30.02	13.08	77.00	5.60	2.19	2.13	16.38	68.79	7.27	3.55	4.02
Counter-current	85.36	30.76	13.69	75.62	5.90	2.22	2.40	14.58	73.34	6.35	2.78	2.94

theoretical investigation of the nanomembrane performance for the nitrogen separation from natural gas. The study examined the performance of the membrane for nominal industrial values of feed conditions. The model also enabled performing useful parametric study of the effect of various operating parameters on the membrane performance, including the effect of feed pressure, permeate pressure as well as flow configuration. The model developed in this study is general and can also be applied to different kinds of nanoporous membrane flow patterns.

Acknowledgments

The authors gratefully acknowledge financial support from King Abdullah Institute for Nanotechnology at King Saud University, Riyadh.

References

Ahmad, F., Keong, L.K., Mun, S.S., Rafiq, S., Khan, A.U., Lee, M., 2015. Hollow fiber membrane model for gas separation: process simulation, experimental validation and module characteristics study. J. Ind. Eng. Chem. 21, 1246–1257. http://dx.doi.org/10.1016/j.jiec.2014.05.041.

Aleklett, K., Höök, M., Jakobsson, K., Lardelli, M., Snowden, S., Söderbergh, B., 2010. The peak of the oil age – analyzing the world oil production reference scenario in world energy outlook 2008. Energy Policy 38, 1398–1414. http://dx.doi.org/10.1016/j.enpol.2009.11.021.

Baker, R.W., 2002. Future directions of membrane gas separation technology. Ind. Eng. Chem. Res. 41, 1393–1411. http://dx.doi.org/10.1021/ie0108088.

Baker, R.W., Lokhandwala, K.A., Wijmans, J.G., Costa, A.R. Da, 2003. Nitrogen removal from natural gas using two types of membranes. U.S. Patent 6,630,011.

Bara, J.E., Gabriel, C.J., Carlisle, T.K., Camper, D.E., Finotello, A., Gin, D.L., Noble, R.D., 2009. Gas separations in fluoroalkyl-functionalized room-temperature ionic liquids using supported liquid membranes. Chem. Eng. J. 147, 43–50. http://dx.doi.org/10.1016/j.cej.2008.11.021.

Bowen, W.R., Welfoot, J.S., 2002. Modelling the performance of membrane nanofiltration-critical assessment and model development. Chem. Eng. Sci. 57, 1121–1137. http://dx.doi.org/10.1016/S0009-2509(01)00413-4.

Cai, J.J., Hawboldt, K., Abdi, M.A., 2012. Contaminant removal from natural gas using dual hollow fiber membrane contactors. J. Memb. Sci. 397–398, 9–16. http://dx.doi.org/10.1016/j.memsci.2011.12.017.

Dionysiou, D.D., 2004. Environmental applications and implications of nanotechnology and nanomaterials. J. Environ. Eng. 130, 723–724. http://dx.doi.org/10.1061/(ASCE)0733-9372(2004)130:7(723).

Fuertes, A.B., 2000. Adsorption-selective carbon membrane for gas separation. J. Memb. Sci. 177, 9–16. http://dx.doi.org/10.1016/S0376-7388(00)00458-0.

Habib, K., Habib, A., 2004. General model of hydrogen transport through nanoporous membranes. Compos. Part B Eng 35, 191–195. http://dx.doi.org/10.1016/j.compositesb.2003.08.007.

Koresh, J.E., Sofer, A., 1983. Molecular sieve carbon permselective membrane. Part I. Presentation of a new device for gas mixture separation. Sep. Sci. Technol. 18, 723–734. http://dx.doi.org/10.1080/01496398308068576.

Lokhandwala, K.A., Pinnau, I., He, Z., Amo, K.D., DaCosta, A.R., Wijmans, J.G., Baker, R.W., 2010. Membrane separation of nitrogen from natural gas: a case study from membrane synthesis to commercial deployment. J. Memb. Sci. 346, 270–279. http://dx.doi.org/10.1016/j.memsci.2009.09.046.

Mulder, M., 1996. Basic Principles of Membrane Technology. Springer Science & Business Media.

Poling, B.E., Prausnitz, J.M., O'connell, J.P., 2001. The Properties of Gases and Liquids, fifth. ed. McGraw-Hill, New York.

Rao, M.B., Sircar, S., 1993a. Nanoporous carbon membrane for gas separation. Gas. Sep. Purif. 7, 279–284. http://dx.doi.org/10.1016/0950-4214(93)80030-Z.

Rao, M.B., Sircar, S., 1993b. Nanoporous carbon membranes for separation of gas mixtures by selective surface flow. J. Memb. Sci. 85, 253–264. http://dx.doi.org/10.1016/0376-7388(93)85279-6.

Rao, M.B., Sircar, S., 1996. Performance and pore characterization of nanoporous carbon membranes for gas separation. J. Memb. Sci. 110, 109–118. http://dx.doi.org/10.1016/0376-7388(95)00241-3.

Rezakazemi, M., Niazi, Z., Mirfendereski, M., Shirazian, S., Mohammadi, T., Pak, A., 2011. CFD simulation of natural gas sweetening in a gas-liquid hollow-fiber membrane contactor. Chem. Eng. J. 168, 1217–1226. http://dx.doi.org/10.1016/j.cej.2011.02.019.

Rufford, T.E., Smart, S., Watson, G.C.Y., Graham, B.F., Boxall, J., Diniz da Costa, J.C., May, E.F., 2012. The removal of CO2 and N2 from natural gas: a review of conventional and emerging process technologies. J. Pet. Sci. Eng. 94–95, 123–154. http://dx.doi.org/10.1016/j.petrol.2012.06.016.

Saidi, M., Heidarinejad, S., Rahimpour, H.R., Talaghat, M.R., Rahimpour, M.R., 2014. Mathematical modeling of carbon dioxide removal using amine-promoted hot potassium carbonate in a hollow fiber membrane contactor. J. Nat. Gas. Sci. Eng 18, 274–285. http://dx.doi.org/10.1016/j.jngse.2014.03.001.

Scholes, C.A., Stevens, G.W., Kentish, S.E., 2012. Membrane gas separation applications in natural gas processing. Fuel 96, 15–28. http://dx.doi.org/10.1016/j.fuel.2011.12.074.

Seo, Y.G., Kum, G.H., Seaton, N.A., 2002. Monte Carlo simulation of transport diffusion in nanoporous carbon membranes. J. Memb. Sci. 195, 65–73. http://dx.doi.org/10.1016/S0376-7388(01)00549-X.

Shindo, Y., Hakuta, T., Yoshitome, H., Inoue, H., 1985. Calculation methods for multicomponent gas separation by permeation. Sep. Sci. Technol. 20, 445–459. http://dx.doi.org/10.1080/01496398508060692.

Soliman, M.A., 1992. A spline collocation method for the solution of diffusion-convection problems with chemical reactions. Chem. Eng. Sci. 47, 4209–4213.

Tagliabue, M., Farrusseng, D., Valencia, S., Aguado, S., Ravon, U., Rizzo, C., Corma, A., Mirodatos, C., 2009. Natural gas treating by selective adsorption: material science and chemical engineering interplay. Chem. Eng. J. 155, 553–566. http://dx.doi.org/10.1016/j.cej.2009.09.010.

Vieira-Linhares, A.M., Seaton, N.A., 2003. Non-equilibrium molecular dynamics simulation of gas separation in a microporous carbon membrane. Chem. Eng. Sci. 58, 4129–4136. http://dx.doi.org/10.1016/S0009-2509(03)00304-X.

Wijmans, J.G., Baker, R.W., 1995. The solution-diffusion model: a review. J. Memb. Sci. 107, 1–21. http://dx.doi.org/10.1016/0376-7388(95)00102-I.

Wu, T., Diaz, M.C., Zheng, Y., Zhou, R., Funke, H.H., Falconer, J.L., Noble, R.D., 2015. Influence of propane on CO_2/CH_4 and N_2/CH_4 separations in CHA zeolite membranes. J. Memb. Sci. 473, 201–209. http://dx.doi.org/10.1016/j.memsci.2014.09.021.

Xu, L., Sedigh, M.G., Tsotsis, T.T., Sahimi, M., 2000. Nonequilibrium molecular dynamics simulation of transport and separation of gases in carbon nanopores. II. Binary and ternary mixtures and comparison with the experimental data. J. Chem. Phys. 112, 910–922. http://dx.doi.org/10.1063/1.480618.

Yildirim, Ö., Kiss, A.A., Hüser, N., Leßmann, K., Kenig, E.Y., 2012. Reactive absorption in chemical process industry: a review on current activities. Chem. Eng. J. 213, 371–391. http://dx.doi.org/10.1016/j.cej.2012.09.121.

Nomenclature

A: membrane area (m^2)
A_T: total membrane area (m^2)
$A_{j,k}$: elements of the matrix of the weights of first derivative
D^K: Knudsen diffusivity (m^2/s)
D_{ij}: binary gas diffusivity (m^2/s)
F: inlet feed flowrate (mol/s)
G: flowrate in permeate (mol/s)
L: membrane thickness (m)
M: mole fractions at the permeate side
N: number of components
n_c: number of collocation points
N: dusty flux (mol/m^2s)
NSD: surface diffusion flux (mol/m^2s)
N_T: total flux through the membrane (mol/m^2s)
P: total pressure inside the membrane (Pa)
P_F: feed pressure (Pa)
P_H: pressure on feed side (Pa)
P_P: pressure on permeate side (Pa)
Q: permeability (mol/s.m.Pa)
r: pore radius (m)
R: universal gas constant (J/mol K)
s: dimensionless relative area
T: temperature (K)
x: mole fraction inside the membrane
X_{interp}: vector of weights of the Lagrange interpolation
y: gas mole fraction at the permeate side
z: dimensionless distance through the membrane

Greek

ε: porosity
μ: gas viscosity (kg/m.s)
τ: turtosity

Subscripts

i,j,k: component index
M: base component
F: feed
H: feed side
P: permeate side